Solid Freeform Fabrication 2023: Proceedings of the 34th Annual International Solid Freeform Fabrication Symposium – An Additive Manufacturing Conference
Reviewed Paper

OPTIMIZATION OF COMPUTATIONAL TIME FOR DIGITAL TWIN DATABASE IN DIRECTED ENERGY DEPOSITION FOR RESIDUAL STRESSES

Usman Tariq[1*], Ranjit Joy[1], Sung-Heng Wu[1], Muhammad Arif Mahmood[2], Michael M Woodworth[3], Frank Liou[1]

[1] Department of Mechanical and Aerospace Engineering, Missouri University of Science and Technology, Rolla, MO 65409, USA.

[2]Intelligent Systems Center, Missouri University of Science and Technology, Rolla, MO 65409, USA.

[3]The Boeing Company, USA

[*] Corresponding author – Email: utariq@mst.edu, Phone: +15733414908, fax: +15733414546, address: 311 Engineering Research Lab, 500 West 16th Street, Rolla, MO, 65409-0440

Abstract

Metal Additive Manufacturing (MAM) has experienced rapid growth and demonstrated its cost-effectiveness in the production of high-quality products. However, MAM processes introduce significant thermal gradients that result in the formation of residual stresses and distortions in the final parts. Finite Element Analysis (FEA) is a valuable tool for predicting residual stresses, but it requires substantial computational power. This study aims to reduce computational time by incorporating a thermo-mechanical model specifically designed for the Directed Energy Deposition (DED) process using Ti6Al4V. This model predicts the thermal history and subsequent residual stresses in the deposited material. Various FEA methods, including "chunk", layer, and conventional methods are examined, providing a comparative analysis of computational cost and numerical accuracy. These findings contribute towards the realization of a digital twin database, where the incorporation of efficient and accurate FEA models can optimize part quality and strength while reducing computational time.

1 Introduction

Additive manufacturing (AM) is a paradigm-shifting manufacturing technique that enables the production of three-dimensional objects through the successive deposition or solidification of material layers [1]. AM permits the direct production of complex structures from computer-generated digital models, unlike conventional subtractive manufacturing techniques, which entail material removal [2]. Typically, this procedure begins with the transformation of a computer-aided design file into a sequence of cross-sectional layers. Depending on the specific process applied, the material is deposited, consolidated, or sintered using AM techniques such as laser powder bed fusion (LPBF), direct energy deposition (DED), fused deposition modeling (FDM), and stereolithography (SLA) [3]. These processes require a variety of materials, including as polymers, metals, ceramics, and composites, which are frequently provided in powder or filament form [3]. The layers are carefully stacked using adhesion techniques like fusion, solidification, or chemical bonding, leading to the construction of complex and useful things. The interdisciplinary nature of AM's scientific foundations enables advances in manufacturing technologies, unique material investigation, and inventive design possibilities [4].

Recently, the scientific world has provided attention towards DED due to its ability to repair worn-out components and produce new ones [5]. In addition, DED allows in-process monitoring and control, allowing modifications to the energy input, deposition rate, and other parameters for best outcomes [5]. In DED, a laser or electron beam is precisely regulated to concentrate its energy on the substrate or previously deposited layer. This energy source rapidly warms the material to the point where it melts or partially melts. The molten material is then precisely placed onto the surface of the target, where it hardens to produce the desired object. Throughout this procedure, the deposition nozzle is often directed along a specified route by the computer-aided design model to guarantee exact material placement [5].

Residual stresses (RSS) play a crucial role in DED processes, exerting a substantial impact on the mechanical behavior and performance of components [6]. During DED, the fast cooling and solidification of the deposited material produce internal tensions that are permanently trapped inside the component. These RSS can cause distortion, warping, and even the beginning of cracks, thus impacting the final product's dimensional accuracy, structural integrity, and functioning [7]. To maintain maximum part quality and performance, it is necessary to comprehend and manage these RSS. To properly assess and minimize residual stressors in DED, a digital twin (DT) technique is necessary [8]. A DT offers a virtual model of the physical system, incorporating real-time process data, material parameters, and sophisticated thermal simulations. By integrating the DT into the DED workflow, manufacturers can correctly estimate and simulate the development of RSS, enabling them to make informed modifications to deposition techniques, energy inputs, and cooling rates [9]. In addition, the DT allows the evaluation of the influence of RSS on component performance via virtual testing, hence aiding the identification of probable failure sites, deformation, and fatigue behavior [10]. Consequently, the DT may serve as a vital instrument for thoroughly comprehending and managing RSS in DED, thereby boosting component quality, structural integrity, and overall production efficiency.

In the context of DED processes, the optimization of computation time is crucial for DTs. DTs in DED entail complex simulations and analysis, which need significant computer resources [11]. Optimization of computation time is vital for the effective and practical application of the DT model. By decreasing calculation time, near-real-time analysis is made possible, allowing for rapid decision-making and improved process management [11]. In the context of DED, where thermal and mechanical simulations are crucial, rapid computation is necessary to assess and optimize deposition strategies, energy inputs, and cooling rates. In addition to facilitating the measurement of RSS, distortion, and component performance, efficient calculation time ensures optimal manufacturing quality [12]. Furthermore, by decreasing calculation time, scalability and practicality are improved, enabling simulations of large-scale components and intricate geometries. This optimization not only increases productivity but also allows for cost savings by decreasing the need for considerable computational resources [13].

To resolve the issues mentioned above, this study proposes chunk and layer methods to compute thermal distribution and residual stresses in a short period, without compromising solution accuracy. The chunk technique is based on the application of a homogeneous body heat flux to a particular portion of the track being deposited, with a thermal load equal to the melting temperature of the deposited material. To provide trustworthiness of the developed technique, experiments were carried out and validated using in-house developed DED machine.

2 Numerical Modelling of DED

In this study, a three-dimensional, implicit, and sequentially coupled, thermo-mechanical model has been developed and applied using the ABAQUS finite element (FE) analysis package to simulate the transient temperature field, and residual stresses during DED process of Ti64Al4V. The numerical modeling consisted of two primary steps. In the first step, a transient thermal analysis was performed to obtain the thermal history across the entire workpiece. In the second step, a mechanical analysis was conducted to determine the residual stress and deformation of the workpiece, using the temperature field data obtained from the previous step [14]. All the simulations were performed in the computer having Intel(R) Xeon(R) W-2295 CPU @ 3.00 GHz equipped with 18 cores and 128 GB RAM at 2934 GHz.

2.1 Thermal Model

During the DED process, the stress and deformation in a structure primarily rely on the temperature field, while the impact of the stress and deformation field on the temperature field is insignificant. As a result, a heat transfer analysis that is decoupled from mechanical effects is deemed appropriate. For thermal analysis, DC3D8 8-nodal linear brick mesh type was used. The transient temperature field, denoted as $T(x, y, z, t)$, spanning the entire domain, was obtained by solving the three-dimensional heat conduction equation (Eq. 1) in the substrate by incorporating the suitable initial and boundary conditions [14]–[17]:

$$\frac{\partial}{\partial x}\left(k\frac{\partial T}{\partial x}\right)+\frac{\partial}{\partial y}\left(k\frac{\partial T}{\partial y}\right)+\frac{\partial}{\partial z}\left(k\frac{\partial T}{\partial z}\right)+Q_v=\rho C_p\frac{\partial T}{\partial t}, \tag{1}$$

where k is the material's thermal conductivity, ρ is material's density, C_P is the material's specific heat, and Q_v is volumetric heat flux. Newton's law of cooling computes for heat loss due to convection is expressed as [14]–[17]:

$$q_c = h_c(T - T_{env}). \tag{2}$$

Here, q_c is the heat loss due to convection, h_c is the convection heat co-efficient, T is surface temperature and T_{env} is the environmental temperature. Heat loss due to radiation is calculated using Stephen-Boltzmann's law [14]–[17]:

$$q_r = \varepsilon\sigma\,(T^4 - T_{env}^4), \tag{3}$$

where q_r is heat loss due to radiation, ε is the emissivity (0.8) and σ is Stephen-Boltzmann's constant (=5.67 × 10^{-8} W/m.K).

2.2 Mechanical Model

Mechanical modeling which is the second step of numerical modelling of DED process can be computed using stress equilibrium, expressed in Eq. 4 [14]–[17]. For mechanical analysis, C3D8 8-node linear brick mesh type was applied.

$$\nabla.\ \sigma + b = 0. \tag{4}$$

Here, ∇ is the divergence operator, σ is stress tensor or Cauchy tensor and b is body forces. All the strains can be divided into two parts: (a) due to mechanical forces, and (b) strain from thermal loads, mentioned in Eq. 5 [14]–[17]. These strains can further be divided into five more strains. Strain caused by elastic, plastic, thermal, phase transformation and transformation of plasticity, compiled in Eq. 6 [14]–[17]. For current analysis, strain due to elastic, plastic and thermal have been considered only, as expressed in Eq. 7 [14]–[17].

$$\varepsilon_{ij} = \varepsilon_{ij}^M + \varepsilon_{ij}^T. \tag{5}$$

In Eq. 5, ε_{ij} is the total strain, ε_{ij}^M is the strain due to mechanical forces, and ε_{ij}^T is the strain due to thermal load.

$$\varepsilon_{ij} = \varepsilon_{ij}^E + \varepsilon_{ij}^P + \varepsilon_{ij}^T + \varepsilon_{ij}^{\Delta V} + \varepsilon_{ij}^{TRP}. \tag{6}$$

In Eq. 6, ε_{ij}^E is the elastic strain, ε_{ij}^P is the strain due to plastic strain, $\varepsilon_{ij}^{\Delta V}$ is strain due to volumetric strain, and ε_{ij}^{TRP} is strain due to phase transformation. Other factors have been disregarded to simplify the numerical analysis.

$$\varepsilon_{ij} = \varepsilon_{ij}^E + \varepsilon_{ij}^P + \varepsilon_{ij}^T. \tag{7}$$

The mechanical constitutive law used in current simulation is defined as [14]–[17]:

$$\sigma = C : \varepsilon^E, \tag{8}$$

where C is the fourth-order elastic stiffness tensor.

3 Methodology and Materials

In this section material details will be presented. Furthermore, experimental setup, and other specifics related to methodology will be discussed.

3.1 Material

In this study, Titanium alloy (Ti6Al4V) is used as it offers numerous advantages in AM. It possesses exceptional strength-to-weight ratio, making it ideal for applications that require lightweight yet robust components. Ti6Al4 exhibits remarkable corrosion resistance, enabling its use in harsh environments. Its biocompatibility makes it suitable for medical and dental implants, ensuring compatibility with the human body. Lastly, Ti6Al4V's compatibility with AM allows for the creation of complex geometries, making it a valuable material for aerospace and automotive industries [18], [19].

To perform FEA, it is essential to have temperature dependent properties to precisely approximate thermal and mechanical behavior. Ti6Al4V's temperature dependent mechanical properties were used in current study [17], as presented in Table 1.

Table 1

Temperature- Dependent material properties of Ti-6Al-4V [17].

Temperature (ºC)	Density (kg/m^3)	Thermal Conductivity (W/m. ºC)	Heat Capacity (J/kg ºC)	Poisson's Ratio	Thermal Expansion Coefficient (µm/m/ ºC)	Young's Modulus (GPa)	Elastic Limit (MPa)
20	4420	7	546	0.345	8.78	110	850
205	4395	8.75	584	0.35	10	100	630
500	4350	12.6	651	0.37	11.2	76	470
995	4282	22.7	753	0.43	12.3	15	13
1100	4267	19.3	641	0.43	12.4	5	5
1200	4252	21	660	0.43	12.42	4	1
1600	4198	25.8	732	0.43	12.5	1	0.5
1650	3886	83.5	831	0.43	12.5	0.1	0.1
2000	3818	83.5	831	0.43	12.5	0.01	0.01

3.2 Experimental Setup

In-house developed DED equipment was used for the following study, which contains neodymium-doped yttrium aluminum garnet optical laser system with 1 kW power. Figure 1a shows the wide view of DED machine system is shown. Figure 1b exhibits the shielding gas system with off-axis powder feeding nozzle along with substrate holder that can move in three dimensions. Figure 1c compiles the specimen built and used in this study along with K-type thermocouples used to extract temperature history to validate numerical model. Two thermocouples, as shown in Figure 1c, were welded using soldering method on to the substrate to extract at with an interval of 0.01 s.

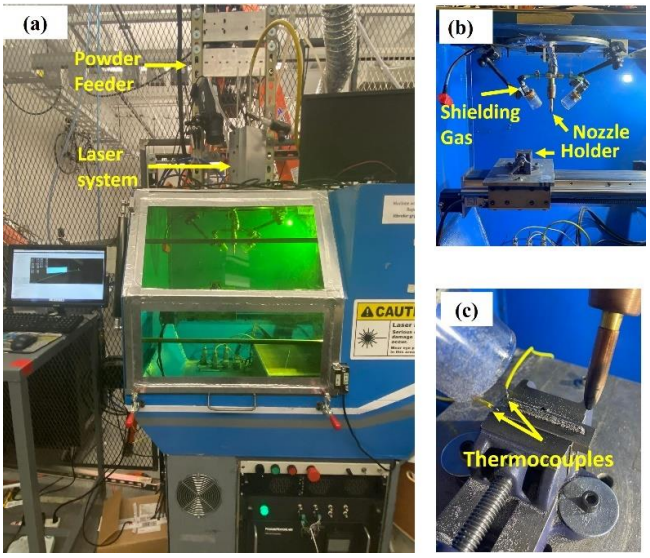

Figure 1. (a) In-house developed DED system, (b) powder and shielding gas system, and (c) built-part along with thermocouples.

For thin wall structure, powder feed rate = 2.0 g/min, Argon shielding gas at pressure = 40 psi with beam spot size = 2.2 mm having Gaussian heat distribution, were utilized. A 6-layered thin wall structure was printed with laser power = 350 W, laser scanning speed = 200 mm/min, and dwell = 0.15 s at the end of each track. Substrate volume was 52 × 12.7 × 6.4 mm^3 while deposit volume was 40 × 2.2 × 3.81 mm^3, each track having 0.6 mm height. Details of thermocouple location and deposit location on the substrate are shown in Figure 2.

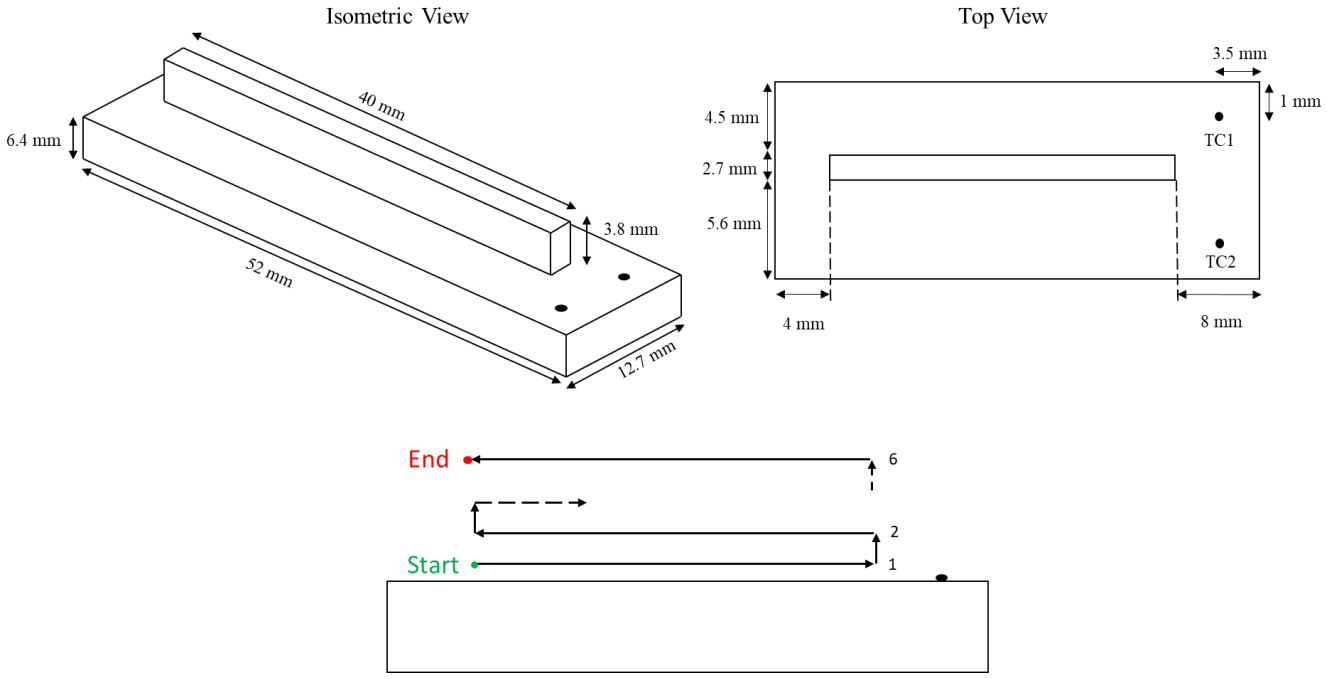

Figure 2. Dimensions of DED Specimen and Scan Strategy

3.3 Thermal Loading and Heat Source

The following assumptions have been made for DED model.

3.3.1 Energy Distribution due to Laser Beam

Goldak's double ellipsoidal heat distribution model was considered. This method utilizes heat source distribution and uses body heat flux at each increment while solving distance equation to move heat source in desired direction with respect to time. Henceforth this method will be called "conventional method."

Due to non-uniform heat source and to capture the resolution of heat source, a smaller element size is required that consequently increases the computational time. It is also worth mentioning here that ABAQUS CAE 2022 includes AM modeler plugin, which solves the Goldak heat source and uses event series to move heat source. For material addition, it uses progressive element activation rather than conventional element birth and death. Above mentioned phenomenon is explained in Figure 3a.

3.3.2 Uniform Distribution of Heat Flux (chunk method)

The concept of the chunk method applies a uniform body heat flux to the portion of the track being deposited, with a thermal load equal to the melting temperature of the deposited material. Body heat flux was applied by calculating the energy input (Q) with respect to scan speed (v), laser power (P), and chunk/layer length (s), absorptivity (a) as shown in Eq. 9 [20].

$$Q = a\frac{s}{v}P \tag{9}$$

One advantage of this method over "layered" or "lumped" methods is that this strategy takes scan pattern into account. Moreover, in terms of adapting this method to the complexity of geometry and consequently tracks, this approach should be applicable to all such geometries. As Abaqus has the functionality to activate elements using 'By Bounding Box' and 'By Bounding Cylinder,' it can accommodate straight and cylindrical tracks, respectively.

Two types of chunk size have been introduced in this study: (a) ½ of track length, and (b) ¼ of track length. Moreover, layer method has also been introduced to compare different thermal loadings in terms of accuracy and computational time. Above mentioned phenomenon is explained in Figure 3b for ¼ of track length.

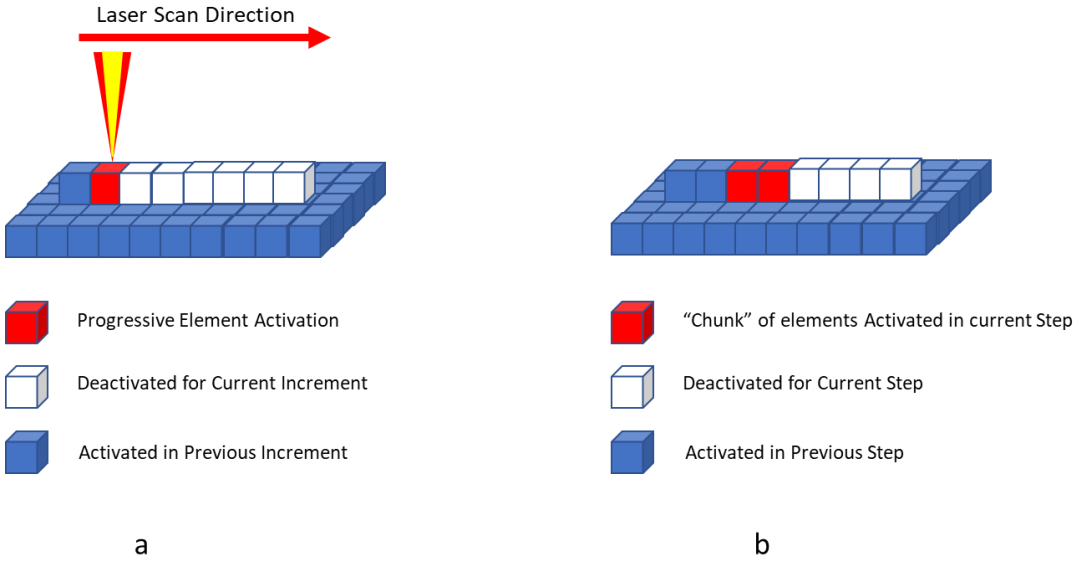

Figure 3. Thermal Load application using (a) energy distribution due to laser heat source, and (b) uniform body heat flux using chunk method.

4 Results and Discussion

This discusses the results and provides discussions on the outcome of this study.

4.1 Thermal Results

Results of the different thermal loading as discussed earlier are compared experimentally using thermocouple in the below section.

4.1.1 Conventional Method

Figures 4a and 4b show a temporal representation of the DED deposition process, demonstrating its evolution across various time intervals. Notably, these results show that the depositing material reaches its specified melting temperature (at least) during printing. This attainment of the melting temperature is critical because it enables proper fusion, in which the molten material solidifies to form a cohesive structure. The results establish a critical relationship between reaching the required temperature and the successful amalgamation of the deposited material, confirming the model's integrity and quality.

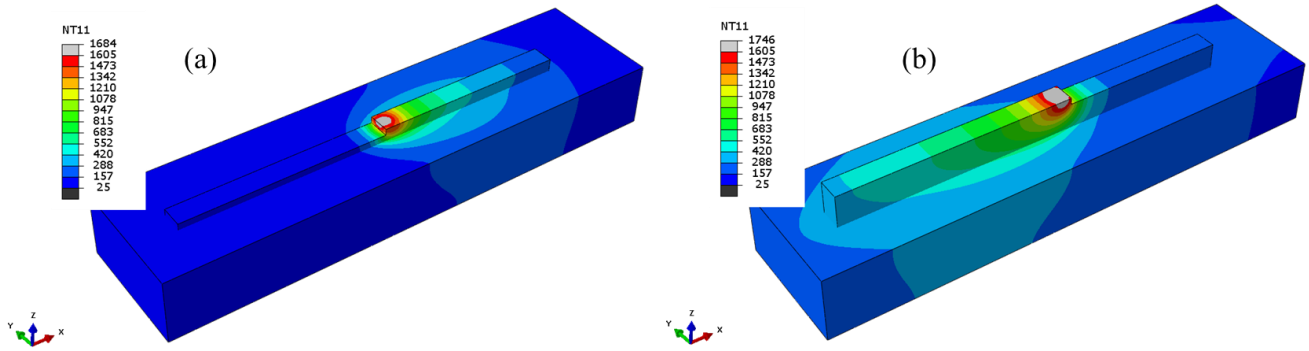

Figure 4. Temperature profile (°C) using conventional method during DED deposition (a) 2nd layer, and (b) 5th layer.

The study's thermal validation includes obtaining nodal values from the same spot where thermocouples were positioned. Figures 5a and 5b show that the acquired results have a satisfactory level of agreement. A notable finding is that thermocouple 1 (TC1) and the accompanying nodes register higher temperatures than thermocouple 2 (TC2). This disparity can be ascribed to the deposition material's proximity to TC1. Due to the shorter distance, heat transfer is more efficient, resulting in higher temperatures detected by TC1 and the related nodes.

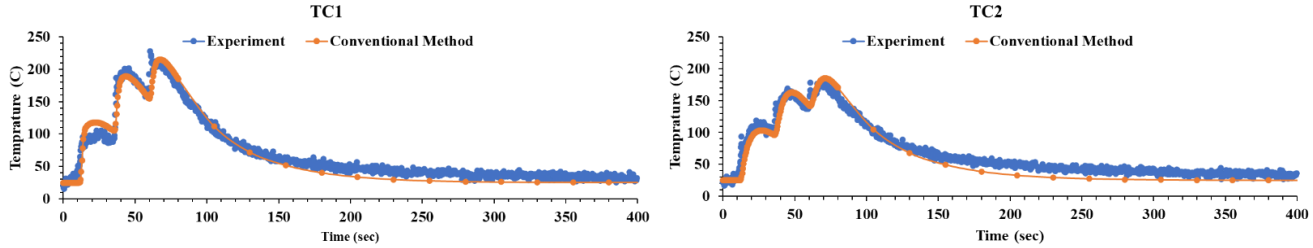

Figure 5 Thermal validation (°C) of conventional method using thermocouple 1 (TC1) and thermocouple 2 (TC2).

4.1.2 Chunk Method

Figure 6 depicts the results obtained using two chunk techniques in the case of 1/4 of track length (a & b) and 1/2 of the track length (c & d). It is clear that material deposition occurred at least the melting temperature in both procedures, ensuring the necessary fusion.

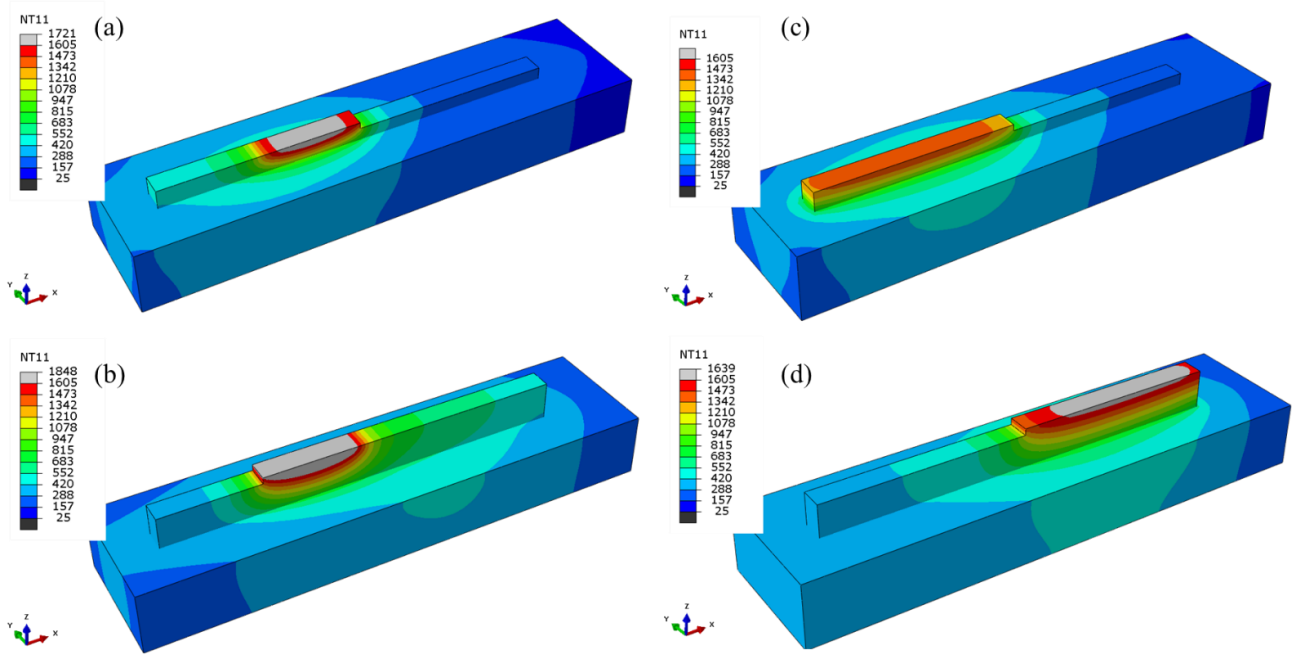

Figure 6. Thermal loading (°C) using chunk method (a) ¼-track-length at 3rd layer & (b) 6th layer, and (c) ½-track-length at 3rd layer & (d) 6th layer.

Thermal validation of these two methods is presented in Figure 7. It can be observed that more accurate results are obtained using smaller chunk size.

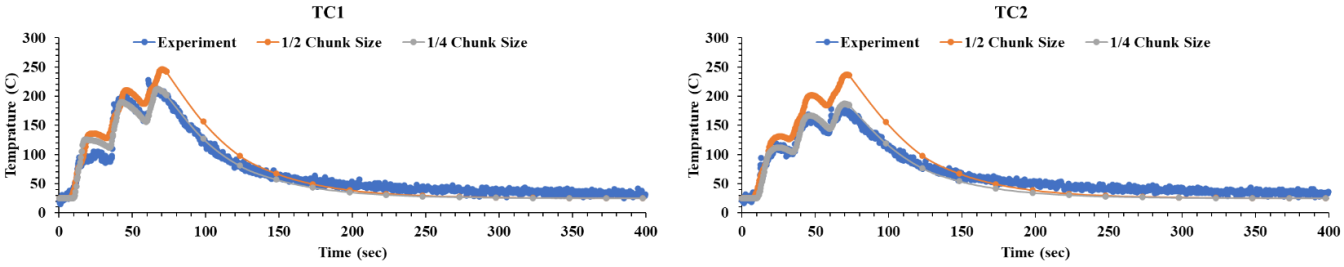

Figure 7 Thermal validation (°C) of chunk Method with thermocouple 1 (TC1) and thermocouple 2 (TC2).

4.1.3 Layer Method

Figure 8 shows the thermal distribution while deposition using layer method. It can be observed that substrate's temperature is very high compared to previous methods. This phenomenon has occurred due to huge amount of load being applied in the form of layering technique whereas in the case of previous methods a small load is applied along with simultaneous cooling.

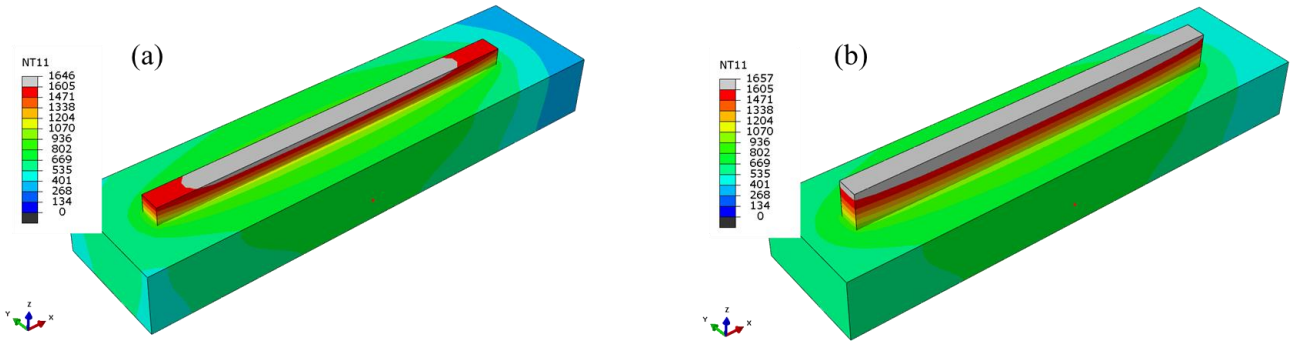

Figure 8. Thermal loading (°C) using layer method at) 3rd, and b) 6th layer.

Nodal values are compared with thermocouple in the form of graphs, as shown in Figure 9. The explanation for the results is the same as Figure 8. It is worth noting that as the chunk size increases, the chunk method gradually moves towards layer method, thus accuracy is decreased significantly.

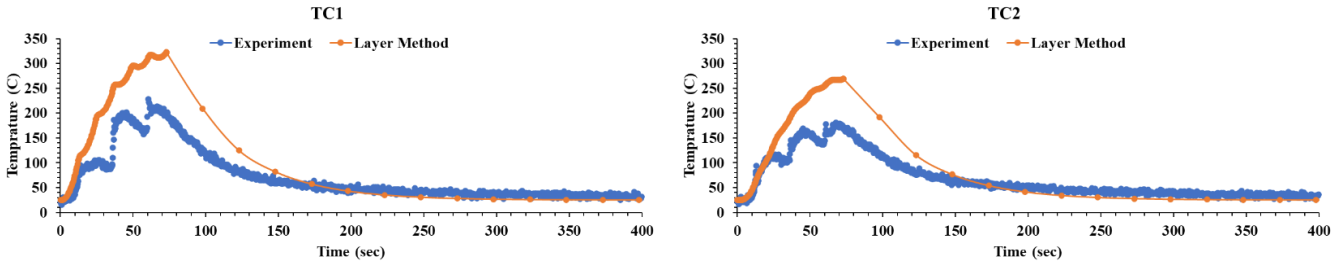

Figure 9. Thermal history (°C) using layer method.

4.2 Residual Stresses

After using thermally calibrated models, residual stresses were calculated by cooling the deposited material up to room temperature in each case. Von-mises stresses calculated by conventional method were equivalent to 2500 MPa, whereas 1/4 chunk, 1/2 chunk and layer method gave residual stresses equivalent to 1500 MPa, 1600 MPa and 1300 MPa, respectively. Even though thermal history of conventional method and 1/4 chunk method, both provided less errors in terms of thermal history but there is still a discrepancy. This discrepancy can be due to the type of heat source used in the simulation. In conventional method, melting area is smaller in the initial layers and increases bigger near the end of deposition, resulting in less residual stresses within the substrate. Whereas for all the other methods, complete melting of whole chunk/layer starts right at the deposition, inducing higher residual stresses within the substrate.

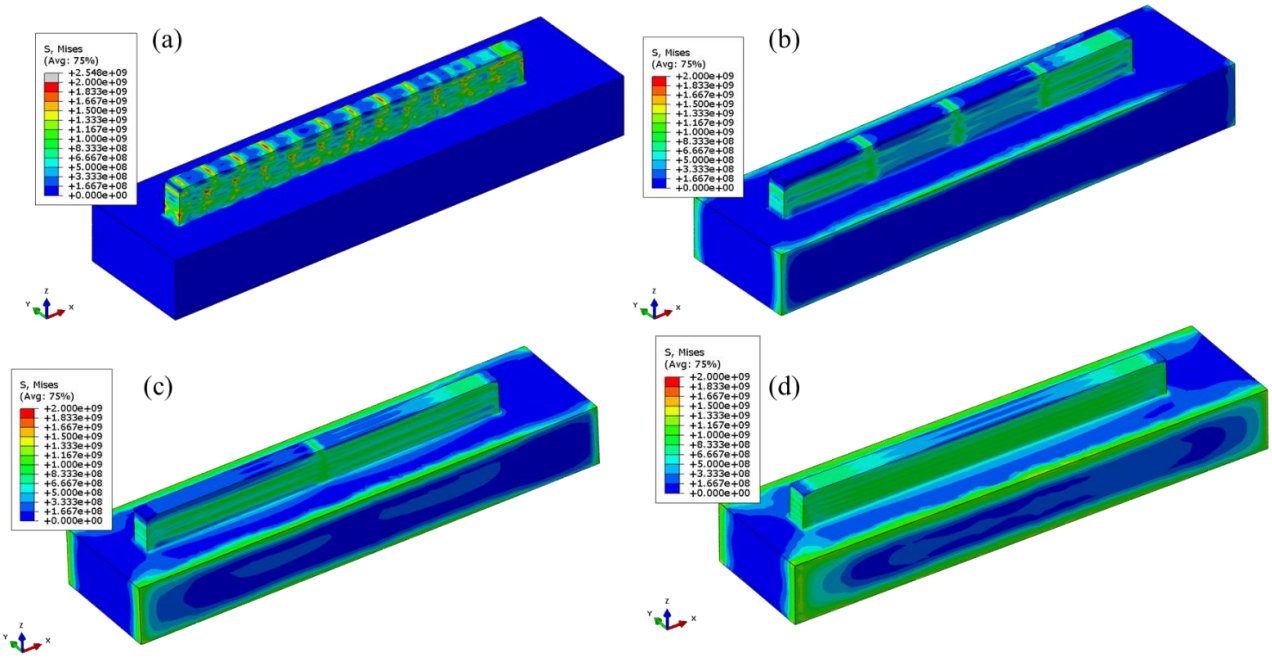

Figure 10 Von-mises stress by (a) conventional method, (b) ¼-track chunk method, (c) ½-track chunk method, and (d) layer method.

4.3 Quantitative Comparison of Different Simulation Methods

The comparison of computational time and error (%) between simulation methods and experimental analysis is shown in Table 2. The error was calculated as:

$$Error\ (\%) = \frac{|x_{exp}^{max} - x_{sim}^{max}|}{x_{exp}^{max}} \times 100. \tag{9}$$

Here, x_{exp}^{max} and x_{sim}^{max} are the maximum temperatures observed by thermocouples and nodes, respectively.

Table 2
Computational Time and Error between different simulations and experimental method.

Simulation Methods	Computational Time = Thermal + Mechanical (mins)	Thermocouple 1 (TC1) error (%)	Thermocouple 2 (TC2) error (%)
Conventional	1041 (756 + 285)	5.7	2.5
1/4 Track chunk Method	113 (51+62)	7.0	3.4
1/2 Track chunk Method	34 (16+18)	7.8	31.3
Layer Method	29 (14+15)	41.4	49.2

5 Conclusion

The goal of this research is to improve computational efficiency by using a thermo-mechanical model customized particularly for the Ti6Al4V Directed Energy Deposition (DED) method. The thermal history and resulting residual stresses within the deposited material can be predicted using this model. The study compares the computational cost and numerical accuracy of multiple Finite Element Analysis methods, including chunk, layer, and traditional methods. The following are the study' s findings:

- When compared to other methods, the chunk method reduces computational time significantly.

- As the layer technique may not be uniformly applicable for estimating thermal history and residual stresses, alternate methods should be investigated in some circumstances.
- Variations in thermal load can cause large changes in the residual stresses of the substrate, stressing the importance of taking such elements into account to effectively quantify and comprehend the ensuing stresses.

In summary, this study emphasizes the benefits of the chunk technique in terms of computational efficiency, the limits of the layer method, and the effect of heat load on residual stresses in the substrate. Moreover, Computational time can see be viewed as a "decision-making tool" when considering the tradeoffs between speed and accuracy in computations and modeling. The ability to get approximate results faster enables more iterative knowledge building and experimentation with imperfect models, a key tenet of the decision making under uncertainty community.

Future Work

Based on the outcome of this study, the following future work has been proposed:

- As residual stress formation is a localized phenomenon; it is essential to have a simulation that is as accurate as the physical phenomenon itself. To ensure its reliability, it is imperative to study a smaller chunk compared to the current study. This should also include the real geometry, with smaller thickness at the start of deposition and greater thickness at the end.
- For this method, Goldak's Ellipsoidal heat source distribution was used. It can be beneficial to show how different types of heat source may work with chunk method especially uniform heat source.
- Residual stresses predicted by conventional and chunk methods need to be validated experimentally to confirm authenticity of newly developed method. Moreover, in-situ and final deformation will also be compared in coming study.

Acknowledgement

This research was partially funded by The Boeing Company, Product Innovation and Engineering (PINE), LLC, NSF Grants CMMI 1625736, NSF EEC 1937128, and Center for Aerospace Manufacturing Technologies (CAMT), Intelligent Systems Center (ISC) and Material Research Center (MRC) at Missouri S&T. Their financial support is greatly appreciated.

References

[1] Y. Fang *et al.*, "Advances in 3D Bioprinting," *Chinese J. Mech. Eng. Addit. Manuf. Front.*, vol. 1, no. 1, p. 100011, Mar. 2022, doi: 10.1016/J.CJMEAM.2022.100011.

[2] R. Galante, C. G. Figueiredo-Pina, and A. P. Serro, "Additive manufacturing of ceramics for dental applications: A review," *Dent. Mater.*, vol. 35, no. 6, pp. 825–846, Jun. 2019, doi: 10.1016/J.DENTAL.2019.02.026.

[3] A. Shrivastava, S. Anand Kumar, S. Rao, B. K. Nagesha, S. Barad, and T. N. Suresh, "Remanufacturing of nickel-based aero-engine components using metal additive manufacturing technology," *Mater. Today Proc.*, vol. 45, pp. 4893–4897, Jan. 2021, doi: 10.1016/J.MATPR.2021.01.355.

[4] Y. Huang, M. C. Leu, J. Mazumder, and A. Donmez, "Additive manufacturing: Current state, future potential, gaps and needs, and recommendations," *J. Manuf. Sci. Eng. Trans. ASME*, vol. 137, no. 1, Feb. 2015, doi: 10.1115/1.4028725/375256.

[5] D. G. Ahn, "Directed Energy Deposition (DED) Process: State of the Art," *Int. J. Precis. Eng. Manuf. Technol. 2021 82*, vol. 8, no. 2, pp. 703–742, Feb. 2021, doi: 10.1007/S40684-020-00302-7.

[6] L. Li, X. Zhang, W. Cui, F. Liou, W. Deng, and W. Li, "Temperature and residual stress distribution of FGM parts by DED process : modeling and experimental validation," pp. 451–462, 2020.

[7] X. Lu *et al.*, “Substrate design to minimize residual stresses in Directed Energy Deposition AM processes,” *Mater. Des.*, vol. 202, p. 109525, Apr. 2021, doi: 10.1016/J.MATDES.2021.109525.
[8] A. Gaikwad, R. Yavari, M. Montazeri, K. Cole, L. Bian, and P. Rao, “Toward the digital twin of additive manufacturing: Integrating thermal simulations, sensing, and analytics to detect process faults,” *https://doi.org/10.1080/24725854.2019.1701753*, vol. 52, no. 11, pp. 1204–1217, Nov. 2020, doi: 10.1080/24725854.2019.1701753.
[9] U. Tariq, R. Joy, . Wu, M. A. Mahmood, A. W. Malik, and F. Liou, “A state-of-the-art digital factory integrating digital twin for laser additive and subtractive manufacturing processes,” *Rapid Prototyp. J.*, 2023, doi: 10.1108/RPJ-03-2023-0113.
[10] L. Chen *et al.*, “Multisensor fusion-based digital twin for localized quality prediction in robotic laser-directed energy deposition,” *Robot. Comput. Integr. Manuf.*, vol. 84, p. 102581, Dec. 2023, doi: 10.1016/J.RCIM.2023.102581.
[11] L. Wright and S. Davidson, “How to tell the difference between a model and a digital twin,” *Adv. Model. Simul. Eng. Sci.*, vol. 7, no. 1, 2020, doi: 10.1186/s40323-020-00147-4.
[12] M. A. Mahmood *et al.*, “Estimation of clad geometry and corresponding residual stress distribution in laser melting deposition: analytical modeling and experimental correlations,” *Int. J. Adv. Manuf. Technol.*, vol. 111, pp. 77–91, Sep. 2020, doi: 10.1007/s00170-020-06047-6.
[13] B. R. Barricelli, E. Casiraghi, and D. Fogli, “A survey on digital twin: Definitions, characteristics, applications, and design implications,” *IEEE Access*, vol. 7, no. Ml, pp. 167653–167671, 2019, doi: 10.1109/ACCESS.2019.2953499.
[14] J. W. Newkirk, “MULTI-LAYER LASER METAL DEPOSITION PROCESS by Presented to the Faculty of the Graduate School of the MISSOURI UNIVERSITY OF SCIENCE AND TECHNOLOGY In Partial Fulfillment of the Requirements for the Degree MASTER OF SCIENCE IN MANUFACTURING ENGINEERING App,” 2014.
[15] X. Lu *et al.*, “Residual stress and distortion of rectangular and S-shaped Ti-6Al-4V parts by Directed Energy Deposition: Modelling and experimental calibration,” *Addit. Manuf.*, vol. 26, no. February, pp. 166–179, 2019, doi: 10.1016/j.addma.2019.02.001.
[16] N. S. Development, D. Additive, and M. Process, “Numerical Simulation Development and,” *Materials (Basel).*, 2020.
[17] X. Lu *et al.*, “Residual stress and distortion of rectangular and S-shaped Ti-6Al-4V parts by Directed Energy Deposition: Modelling and experimental calibration,” *Addit. Manuf.*, vol. 26, pp. 166–179, 2019, doi: https://doi.org/10.1016/j.addma.2019.02.001.
[18] W. Liu, Y. Lin, Y. Chen, T. Shi, and A. Singh, “Effect of Different Heat Treatments on Microstructure and Mechanical Properties of Ti6Al4V Titanium Alloy,” *Rare Met. Mater. Eng.*, vol. 46, no. 3, pp. 634–639, Mar. 2017, doi: 10.1016/S1875-5372(17)30109-1.
[19] E. Akman, A. Demir, T. Canel, and T. Sinmazçelik, “Laser welding of Ti6Al4V titanium alloys,” *J. Mater. Process. Technol.*, vol. 209, no. 8, pp. 3705–3713, Apr. 2009, doi: 10.1016/J.JMATPROTEC.2008.08.026.
[20] K. Salonitis, L. D’Alvise, B. Schoinochoritis, and D. Chantzis, “Additive manufacturing and post-processing simulation: laser cladding followed by high speed machining,” *Int. J. Adv. Manuf. Technol.*, vol. 85, no. 9–12, pp. 2401–2411, 2016, doi: 10.1007/s00170-015-7989-y.